

UNVEILING THE SECRETS OF METALLICITY AND MASSIVE STAR FORMATION USING DLAS ALONG GAMMA-RAY BURSTS

A. CUCCHIARA¹, M. FUMAGALLI^{2,3}, M. RAFELSKI¹, D. KOCEVSKI¹, J. X. PROCHASKA⁴, R. J. COOKE⁴, AND G. D. BECKER⁵

¹NASA Postdoctoral Program Fellow, Goddard Space Flight Center, Greenbelt, MD 20771, USA; antonino.cucchiara@nasa.gov

²Institute for Computational Cosmology, Department of Physics, Durham University, South Road, Durham, DH1 3LE, UK

³Carnegie Observatories, 813 Santa Barbara Street, Pasadena, CA 91101, USA

⁴Department of Astronomy and Astrophysics, UCO/Lick Observatory, University of California, 1156 High Street, Santa Cruz, CA 95064, USA

⁵Kavli Institute for Cosmology and Institute of Astronomy, University of Cambridge, Madingley Road, Cambridge, CB3 0HA, UK

Received 2014 August 12; accepted 2015 February 17; published 2015 April 30

ABSTRACT

We present the largest, publicly available sample of damped Ly α systems (DLAs) along the lines of sight of *Swift*-discovered gamma-ray bursts (GRBs) in order to investigate the environmental properties of long GRB hosts in the $z = 1.8$ – 6 redshift range. Compared with the most recent quasar DLA sample (QSO-DLA), our analysis shows that GRB-DLAs probe a more metal-enriched environment at $z \gtrsim 3$, up to $[X/H] \sim -0.5$. In the $z = 2$ – 3 redshift range, despite the large number of lower limits, there are hints that the two populations may be more similar (only at a 90% significance level) than at higher redshifts. Also, at high- z , the GRB-DLA average metallicity seems to decline at a lower rate than the QSO-DLAs: GRB-DLA hosts may be polluted with metals at least as far as ~ 2 kpc from the GRB explosion site, probably due to previous star formation episodes and/or supernova explosions. This shallow metallicity trend, now extended up to $z \sim 5$, confirms previous results that GRB hosts are star-forming and have, on average, higher metallicities than the general QSO-DLA population. Finally, our host metallicity measurements are broadly consistent with the predictions derived from the hypothesis of two channels of GRB progenitors, one of which is mildly affected by a metallicity bias, although more data are needed to constrain the models at $z \gtrsim 4$.

Key words: galaxies: general – galaxies: ISM – gamma-ray burst: general – quasars: absorption lines – techniques: imaging spectroscopy

1. INTRODUCTION

One of the fundamental aspects of the formation of the first stars and galaxies is the actual conversion of the primordial hydrogen clouds into the first massive, almost metal-free, objects (such as a Population III star; Barkana & Loeb 2001). This first generation of stars, at $z \gtrsim 10$, disappeared quite rapidly due primarily to strong negative feedback effects (Yoshida et al. 2008; Greif et al. 2012; Bromm 2013; Karlsson et al. 2013; Chen et al. 2015). However, some of these objects and the subsequent generation of stars probably ended their lives in very energetic explosions, either as pair-instability supernovae (PISNe) or as long Gamma-Ray Bursts (GRBs; see Meszáros 2013 for a review), which can be detected by current and future high-energy missions up to the highest redshifts.

Thanks to the *Swift* satellite (Gehrels et al. 2004), hundreds of GRBs have been discovered, even up to $z \approx 8$ (Salvaterra et al. 2009; Tanvir et al. 2009; Cucchiara et al. 2011b). These high- z GRBs can be used to test cosmic star formation rate models as well as the cosmological chemical enrichment (Kistler et al. 2009; Robertson & Ellis 2012; Salvaterra et al. 2012; Tanvir et al. 2012; Ritter et al. 2014). GRB progenitor models require massive, fast-rotating, and low-metallicity objects (Woosley 1993; Galama et al. 1998; Hjorth et al. 2003b; Berger et al. 2011; Woosley 2011; Levan et al. 2014), though the discovery of a few GRBs that might have occurred in a solar or even super solar metallicity environment challenges this paradigm (e.g., Prochaska et al. 2009; Krühler et al. 2012; Savaglio 2012).

Afterglow absorption spectroscopy of $z \gtrsim 1.5$ GRBs provides a unique tool to determine the constituents of the GRB environment, in particular the amount of metals produced

by past and ongoing star formation in the vicinity of the GRB explosion. This has important consequences for our understanding of the progenitor itself as well as the galaxies hosting GRBs throughout cosmic time. GRBs are identified, at first, based only on their high energy emission; therefore, their hosts can be studied in great detail after the afterglow emission disappears, representing a sample of star-forming galaxies unbiased with respect to their intrinsic luminosity. In fact, it is possible to use GRBs and their hosts to trace cosmic star formation independently compared to magnitude-limited Lyman-break galaxy surveys, although the effects of dust and metallicity biases are still under investigation (Modjaz et al. 2008; Levesque et al. 2010; Kocevski & West 2011; Trenti et al. 2013; Bouwens et al. 2014; Trenti et al. 2014).

Similar to GRBs, quasars (QSOs) have also been used for decades to study the effects of re-ionization, the conversion of neutral hydrogen into stars, and the cosmic metal enrichment. In fact, QSOs, like GRB optical afterglows, are very bright and can be seen up to very high redshift. The spectra of QSOs often show the presence of intervening absorbers (at redshifts lower than the QSOs), some of which are associated with large reservoirs of neutral hydrogen along their LOSs. In particular, Damped Ly α systems (DLAs), by definition, have the column density of neutral hydrogen $N_{\text{H I}} \geq 22 \times 10^{20} \text{ cm}^{-2}$, while sub-DLAs are defined as absorbers with column density $10^{19} < N_{\text{H I}} < 22 \times 10^{20} \text{ cm}^{-2}$ (other types of subdivisions have been made, but they are not relevant for the purpose of this work). These absorbers, which often trace galaxies along the QSO LOS (e.g., Fynbo et al. 2011; Schulze et al. 2012), are the best laboratories to investigate the ISM, its evolution, and cosmic star formation at high redshift, providing important constraints on galaxy evolution models (e.g., Wolfe et al. 2005;

Fynbo et al. 2011; Rafelski et al. 2012; Krogager et al. 2013; Neeleman et al. 2013; Christensen et al. 2014; Fumagalli et al. 2014; Jorgenson & Wolfe 2014).

Recently, Rafelski et al. (2014) have extended QSO-DLA studies up to $z \sim 5$: they showed that the overall cosmological mean metallicity⁶ slowly decreases from $z \approx 1$ up to $z \approx 4.7$ (see also Prochaska et al. 2003; Rafelski et al. 2012; Jorgenson et al. 2013) and then it appears to drop rapidly below the extrapolated linear metallicity evolution, as if a sudden metallicity enrichment in DLAs occurred shortly after the end of re-ionization. GRB-DLAs, in which the DLA is inside the GRB host, have been sparsely studied (Fynbo et al. 2008b; Savaglio 2012; Sparre et al. 2013; Arabalmani et al. 2015), mainly due to the small sample size, the different data quality, and incompleteness. Nevertheless, Prochaska et al. (2007) have derived a higher metal content at $z \gtrsim 2$ for a set of GRB-DLAs with respect to a large sample of QSO-DLAs, suggesting that GRBs probe denser, more dust-depleted, and metal-rich regions than the QSO-DLAs population (see also Fynbo et al. 2013).

Finally, chemical evolution models suggest that DLA metallicity measurements and relative abundance ratios at very high- z will enable us to better understand the effect of the primordial PopIII stars' chemical enrichment (and initial mass function (IMF)) on subsequent PopII stars' IMF (Salvadori & Ferrara 2012; Kulkarni et al. 2013; Ritter et al. 2014).

The goal of this study is twofold: (1) compare the findings by (Rafelski et al. 2014), hereafter R14, with a large sample of GRB-DLAs that extends previous studies (Prochaska et al. 2007; Savaglio 2012; Arabalmani et al. 2015); and (2) investigate the metallicity evolution of GRB-DLAs and compare it with host galaxy metallicity predictions at different redshifts.

The paper is structured as follows: in the next section we will present our samples of GRB- and QSO-DLAs, in Section 3 we will describe our analysis, in Section 4 we will discuss our findings and possible biases, and in Section 5 we will summarize our results. Throughout the paper we adopt the solar metallicity measurements from Asplund et al. (2009), with solar abundance of $[X/H]_{\odot}$ equal to 7.12 (sulfur), 7.51 (silicon), and 4.56 (zinc).

2. SAMPLES

2.1. GRB DLAs

We select our GRB-DLA sample from all the GRB afterglows observed during the 2000–2014 time span for which H I and metallicity measurements can be obtained (Table 1). In order to detect the Ly α absorption line (1216 Å rest-frame) with most of the current spectrographs, a GRB has to be at least at $z \sim 1.8$ in order for the line to be redshifted out of the atmospheric blue cut-off (which usually means a minimum observed wavelength limit of ~ 3400 Å). GRB-DLA absorbers are unambiguously associated with GRB host galaxies, since often fine-structure transitions (e.g., Fe II* $\lambda 2316$) or the termination of the Ly α forest are identified at the same redshift as the Ly α feature (Prochaska et al. 2006; Vreeswijk et al. 2007). The presented sample includes spectra obtained with different instrument resolutions: from low

resolution (resolving power $R \sim 400$) spectra obtained with the AIFOSC camera, to high resolution ($R \sim 55,000$) spectra obtained with the UVES instrument. Due to the transient nature of GRB afterglows, some spectra were obtained when the afterglow was quite faint and the resulting signal-to-noise ratio (S/N) of the acquired spectra is not uniform within the sample. We therefore exclude GRBs with $S/N \leq 3$ (at usually 6000 Å) due to the unreliable detection of metal lines (see Section 3). All the data obtained with the Very Large Telescope (VLT) instruments were retrieved from the ESO Archive⁷ or were available within our collaboration.⁸ In a few cases we could not obtain the raw data and we included the results from abundance analysis as they appeared in the literature (e.g., GRB 050904 obtained with the FOCAS camera on the Subaru telescope). We include these systems in Table 1 and briefly describe each line of sight (LOS) in Appendix.

Our sample includes 13 GRB afterglow spectra obtained with the X-Shooter instrument mounted on the VLT. In order to analyze these data we primarily use our own customized pipeline written in IDL (G. D. Becker et al. 2015, private communication) as it is optimized for point sources and has an improved sky subtraction procedure. Additionally, we used the official pipeline (version 2.5, within the REFLEX workflow (Goldoni et al. 2006; Freudling et al. 2013) to verify the output of our custom pipeline. For completeness, in the last column of Table 1 we report the literature reference where these data, if published, appear.

Among the GRBs in Table 1 there are 12 sub-DLAs and we exclude them from subsequent analysis due to the fact that these absorbers may probe a different environment than the general DLA population. These objects will be studied in a companion paper (A. Cucchiara et al. 2015, in preparation), where we will present a more detailed description of the ionization field in order to reproduce the observed absorption pattern (see, for example, Vreeswijk et al. 2013). We also exclude four GRBs where only upper limits on the $N_{\text{H I}}$ could be placed (GRB 071020, GRB 051111, GRB 080913, and GRB 090323), but we report them for completeness. For four other GRB-DLAs only $N_{\text{H I}}$ measurement was obtained but the S/N is too low to reliably identify any metal feature (GRB 020124, GRB 060522, GRB 080603B, and GRB 121201A). In summary our GRB-DLA sample is comprised of 55 GRB-DLA LOS (3 from the literature). Among these 55, we present metal abundances for 11 new GRB-DLA LOSs.

2.2. Quasar DLAs

Thanks to the Sloan Digital Sky Survey large samples of quasars have been obtained up to $z \sim 7$. Thousands of these QSOs present DLAs along their LOS. We use the current most complete list of high-resolution QSO-DLA spectra obtained by Rafelski et al. (2012, hereafter R12), and R14, which extend previous work from, e.g., Prochaska et al. (2003). All these QSOs have been observed with high-resolution spectrographs and have very high S/N, which are of great importance in order to resolve multiple narrow metal feature (see also Section 3.1) as well as to provide accurate metallicity measurements using different metal tracers.

⁶ The cosmic mean metallicity is defined as $\langle Z \rangle = \log \left(\frac{\sum_i 10^{[M/H]_i} N(\text{H I})_i}{\sum_i N(\text{H I})_i} \right)$, where i is the redshift bin of DLAs as a function of redshift.

⁷ Based on data obtained from the ESO Science Archive Facility.

⁸ <http://grbspecdb.ucolick.org/>

Table 1
RB-DLAs Sample

GRB	z_{GRB}	$\log(N_{\text{H I}})$	$[X/H]^a$	Ion	Fine-structure	Telescope/ Instrument	Resolution at 6000Å	S/N per Pixel	Reference
000926	2.3621	21.3 ± 0.25	≥ -0.30	Zn	N	Keck/ESI	20,000	10	(1)
011211	2.1427	20.4 ± 0.2	≥ -1.22	Si	N	VLT/FORS2	2400	10	(2)
020124	3.198	21.7 ± 0.2	N	VLT/FORS1	450	4	(3)
021004	2.3289	19.0 ± 0.2	Y	VLT/UVES	40000	6	(4)(5)
030226	1.98	20.5 ± 0.3	≥ -1.28	Fe	Y	Keck/ESI	20000	40	(6)
030323	3.3714	21.9 ± 0.07	≥ -1.32	S	Y	VLT/FORS2	2100	20	(7)
030429	2.658	21.6 ± 0.2	≥ -1.13	Si	N	VLT/FORS1	600	40	(8)
050319	3.24	20.9 ± 0.2	$> -0.77^c$	S	N	NOT/AIFOSC	355	4	(9)(10)
050401	2.899	22.6 ± 0.3	≥ -1.07	Zn	Y	VLT/FORS2	545	10	(11)
050505	4.27	22.05 ± 0.1	≥ -1.2	S	Y	Keck/LRIS	1200	20	(12)
050730	3.96723	22.1 ± 0.1	-1.96 ± 0.11	S	Y	VLT/UVES	40000	10	(13)(14)
050820A	2.6145	21.1 ± 0.1	-0.76 ± 0.13	S	Y	VLT/UVES	40000	12	(8)
			-0.78 ± 0.11	Fe	Y	Keck/HIRES	30000	10	(14)
050904	6.26	21.3 ± 0.2	$\geq -1.0^c$	S	Y	Subaru/FOCAS	1000	7	(15)
050908	3.344	19.4 ± 0.2	N	Gemini/GMOS	1200	20	(16)
050922C	2.1996	21.55 ± 0.1	-1.88 ± 0.14	S	Y	VLT/UVES	45000	10	(17)
051111	1.549	<21.9	Y	Keck/HIRES	55000	20	(18)
060115	3.533	21.5 ± 0.1	> -1.53	S	Y	VLT/FORS1	990	4	(9)
060124	2.3	18.5 ± 0.5	N	Keck/LRIS	1200	18	(9)
060206	4.048	20.85 ± 0.1	≥ -0.74	S	Y	Lick/KAST	1200	28	(9)
060210	3.913	21.55 ± 0.15	≥ -0.83	Si	Y	Gemini/GMOS	1200	40	(9)
060223A	4.41	21.6 ± 0.1	$> -1.8^c$	S	N	Keck/LRIS	1200	...	(19)
060510B	4.94	21.3 ± 0.1	≥ -0.84	S	N	Gemini/GMOS	1200	15	(19)
060522	5.11	21.0 ± 0.3^c	N	Keck/LRIS	1200	2	(19)
060526	3.221	19.9 ± 0.15	N	VLT/FORS1	1200^b	18	(20)
060605	3.773	18.9 ± 0.4	Y	PMAS	500	7	(21)
060607A	3.075	16.95 ± 0.03	Y	VLT/UVES	55000	30	(17)
060707	3.425	21.0 ± 0.2	≥ -1.69	Fe	Y	VLT/FORS2	800	7	(22)
060714	2.711	21.8 ± 0.1	≥ -0.97	Zn	Y	VLT/FORS1	800	30	(22)
060906	3.686	21.85 ± 0.10	≥ -1.72	S	N	VLT/FORS1	800	8	(22)
060926	3.206	22.6 ± 0.15	≥ -1.32	Zn	Y	VLT/FORS1	800	20	(22)
060927	5.464	22.50 ± 0.15	≥ -1.55	S	N	VLT/FORS1	500	3	(23)
061110B	3.433	22.35 ± 0.10	≥ -1.84	S	Y	VLT/FORS1	800	10	(9)
070110	2.351	21.7 ± 0.1	≥ -1.32	Si	Y	VLT/FORS2	800	15	(9)
070411	2.954	19.3 ± 0.3	Y	VLT/FORS2	800	8	(9)
070506	2.308	22.0 ± 0.3	≥ -0.65	Zn	N	VLT/FORS1	800	18	(9)
070721B	3.628	21.5 ± 0.2	≥ -2.14	Si	Y	VLT/FORS2	800	5	(9)
070802	2.455	21.5 ± 0.2	≥ -0.54	Si	Y	VLT/FORS2	800	7	(9)
071020	2.145	<20.30	N	VLT/FORS2	800	5	(9)
071031	2.692	22.15 ± 0.05	-1.85 ± 0.12	Fe	Y	VLT/UVES	55000	10	(24)
080210	2.641	21.9 ± 0.1	≥ -1.37	Fe	Y	VLT/FORS2	1400	25	(9)(25)
080310	2.427	18.7 ± 0.1	Y	VLT/UVES	55000	30	(17)
080413A	2.433	21.85 ± 0.15	≥ -1.56	Zn	N	Gemini/GMOS	1200	17	(24)
080603B	2.69	21.85 ± 0.05^c	Y	NOT/AIFOSC	355	...	(9)
080607	3.037	22.7 ± 0.15	≥ -1.72	Fe	Y	Keck/LRIS	2000	40	(9)(26)
080721	2.591	21.6 ± 0.1	≥ -1.73	S	N	VLT/FORS1	800	40	(27)
080804	2.20542	21.3 ± 0.1	-0.75 ± 0.16	Zn	N	VLT/UVES	55000	10	(9)
			$\gtrsim -1.25$	Zn	N	Gemini	1200	10	(10)
080810	3.35	17.5 ± 0.15	Y	NOT/AIFOSC	400	8	(28)
			Y	Keck/HIRES	50000	30	(28)
080913	6.69	<19.84	N	VLT/FORS2	800	3	(29)
081008	1.96	21.59 ± 0.1	-0.86 ± 0.14	S	Y	VLT/UVES	40000	5	(30)
			≥ -1.41	S	Y	Gemini/GMOS	1200	12	this work
090205	4.64	20.73 ± 0.05	> -0.57	S	Y	VLT/FORS1	440	5	(31)
090323	3.5778	>19.90	Y	VLT/FORS2	1200	24	(32)(33)
090426	2.609	19.1 ± 0.15	N	Keck/LRIS	1200	7	(20)
090516	4.109	21.73 ± 0.1	≥ -1.36	Si	Y	VLT/FORS2	800	70	(34)
090809	2.73	21.40 ± 0.08	-0.57 ± 0.10	Si	Y	VLT/X-Shooter	8000	12	(35)
090812	2.425	22.3 ± 0.1	≥ -1.64	Si	Y	VLT/FORS2	800	60	(36)
090926A	2.1062	21.73 ± 0.07	≈ -1.9	S	Y	VLT/FORS2	780	35	(37)

Table 1
(Continued)

GRB	z_{GRB}	$\log(N_{\text{H1}})$	$[X/H]^a$	Ion	Fine-structure	Telescope/ Instrument	Resolution at 6000Å	S/N per Pixel	Reference
100219A	4.667	21.13 ± 0.12	-2.18 ± 0.12	S	Y	VLT/X-Shooter	10000	20	(37)
			-0.95 ± 0.18	S	Y	VLT/X-Shooter	6000	6	(38)
			≥ -1.8	S	Y	Gemini/GMOS	1200	7	this work
100425A	1.755	21.05 ± 0.10	-0.96 ± 0.42	Fe	Y	VLT/X-Shooter	8000	4	(35)
110205A	2.214	21.45 ± 0.2	≥ -0.82	S	Y	FAST	2400	30	(39)
111008A	4.98968	22.3 ± 0.06	-1.63 ± 0.13	Fe	Y	VLT/X-Shooter	10000	10	(40)
111107A	2.893	21.0 ± 0.10	≥ -0.45	S	Y	VLT/X-Shooter	8000	5	this work
120327A	2.813	22.01 ± 0.09	-1.51 ± 0.11	S	Y	VLT/X-Shooter	8000	30	(41)
120716A	2.487	21.55 ± 0.15	≥ -1.76	Fe	Y	VLT/X-Shooter	8000	7	this work
120815A	2.3574	21.95 ± 0.1	-0.93 ± 0.13	Zn	Y	VLT/X-Shooter	10000	12	(42)
120909A	3.9293	21.20 ± 0.10	-0.66 ± 0.11	S	Y	VLT/X-Shooter	8000	9	this work
121024A	2.2977	21.50 ± 0.10	-0.40 ± 0.12	Zn	Y	VLT/X-Shooter	8000	15	(43)
121201A	3.385	21.7 ± 0.2	VLT/X-Shooter	8000	$\lesssim 3$	this work
130408A	3.757	21.70 ± 0.10	-1.24 ± 0.12	S	Y	VLT/X-Shooter	8000	50	this work
			≥ -1.1	S	Y	Gemini/GMOS	1200	20	this work
130505A	2.2687	20.65 ± 0.10	≥ -1.42	Fe	Y	Gemini/GMOS	1200	30	this work
130606A	5.9134	19.93 ± 0.2	Y	Gemini/GMOS	1200	...	(44)
140226A	1.9733	20.60 ± 0.20	≥ -0.54	Fe	N	keck/LRIS	1200	30	this work
140311A	4.953	21.80 ± 0.30	≥ -1.65	Ni	Y	Gemini/GMOS	1200	7	this work
140419A	3.961	19.3 ± 0.2	Y	Gemini/GMOS	1200	20	this work
140423A	3.258	20.45 ± 0.20	≥ -1.44	Fe	Y	Gemini/GMOS	1200	20	this work
140518A	4.7055	21.65 ± 0.20	≥ -1.06	S	Y	Gemini/GMOS	1200	50	this work

Notes. List of the GRB-DLAs identified to date along GRB lines of sight. Missing metallicities are due to a lack of metal line transitions or the low signal-to-noise of the spectra. When multiple measurements for the same line of sight are listed, the one derived from the high resolution instrument is adopted in our analysis. Some values, either of N_{H1} or $[X/H]$, are adopted from the literature reference listed in the last column.

References. (1) Castro et al. (2003), (2) Vreeswijk et al. (2006), (3) Hjorth et al. (2003a), (4) Savaglio et al. (2002), (5) Fiore et al. (2005), (6) Shin et al. (2006), (7) Vreeswijk et al. (2004), (8) Jakobsson et al. (2004), (9) Fynbo et al. (2009), (10) Laskar et al. (2011), (11) Watson et al. (2006), (12) Berger et al. (2006), (13) D’Elia et al. (2007), (14) Prochaska et al. (2007), (15) Kawai et al. (2006), (16) Chen et al. (2007), (17) Fox et al. (2008), (18) Penprase et al. (2006), (19) Chary et al. (2007), (20) Thöne et al. (2010), (21) Ferrero et al. (2009), (22) Jakobsson et al. (2006), (23) Ruiz-Velasco et al. (2007), (24) Ledoux et al. (2009), (25) de Cia et al. (2011), (26) Prochaska et al. (2009), (27) Starling et al. (2009), (28) Page et al. (2009), (29) Patel et al. (2010), (30) D’Elia et al. (2011), (31) D’Avanzo et al. (2010), (32) Cenko et al. (2011), (33) Savaglio (2012), (34) de Ugarte Postigo et al. (2012), (35) Skùladóttir (2010), (36) Rau et al. (2010), (37) D’Elia et al. (2010), (38) Thöne et al. (2013), (39) Cucchiara et al. (2011a), (40) Sparre et al. (2014), (41) D’Elia et al. (2014), (42) Krühler et al. (2013), (43) Friis et al. (2014), (44) Chornock et al. (2013).

^a Metallicities are relative to solar: $[X/H] = \log[X/H]_{\text{DLA}} - \log[X/H]_{\odot}$. For sub-DLA systems, with $10^{19} < N_{\text{H1}} < 2.2 \times 10^{20} \text{ cm}^{-2}$, we defer this to a future paper.

^b Average over multiple spectra; see the Appendix.

^c Value reported in the literature.

3. ANALYSIS

Our data set allows us to assess ionic metal abundances directly from the afterglow spectra rather than relying on the literature. First, we select the spectra obtained with high-resolution spectrographs (which we defined at $R \gtrsim 6000$; see also Jorgenson et al. 2013) and high S/N, and compare them to the QSO-DLA sample that has been obtained with high-resolution instruments only (e.g., HIRES on the Keck telescopes). Second, as already presented by Prochaska (2006), abundance estimates (as well as the associated statistical error) obtained using low-resolution spectrographs are often underestimated because of saturation effects while blending may cause an overestimation, and therefore the measurements should be used with caution. As mentioned before, we perform our own analysis for the GRB LOSs and, in the following sections, we discuss in detail our results from the low-resolution sample. Our approach yields a more homogeneous sample, similar to the QSO-DLA sample, for which the same procedure has been applied.

3.1. Low Resolution Sample

The consequences of low-resolution ($R \lesssim 6000$) spectroscopy on GRB-DLA abundance measurements via, e.g., Curve of Growth methodology (COG; Spitzer 1978) has already been discussed in the literature (Prochaska 2006; Jorgenson et al. 2013). Our large and diverse sample enables us to directly compare abundance measurements obtained for systems with different intrinsic metallicity. In the first column of Figures 1 and 2 we show line profiles for two systems observed with the VLT/UVES instrument, which provides a resolution of 7 km s^{-1} (left column): GRB 050820A (Figure 1) is a GRB-DLA with intrinsic moderate metallicity ($Z/Z_{\odot} = -0.76$), while GRB 050730 is a metal-poor system ($Z/Z_{\odot} = -1.96$). In the second and third columns we present the same spectra resampled at the resolution of our average X-Shooter and Gemini/GMOS instruments, respectively. Three important effects are evident and require particular attention when estimating abundances with mid/low-resolution instruments: (1) blending of nearby lines, either from other transitions rising from the GRB-DLA system or from unrelated

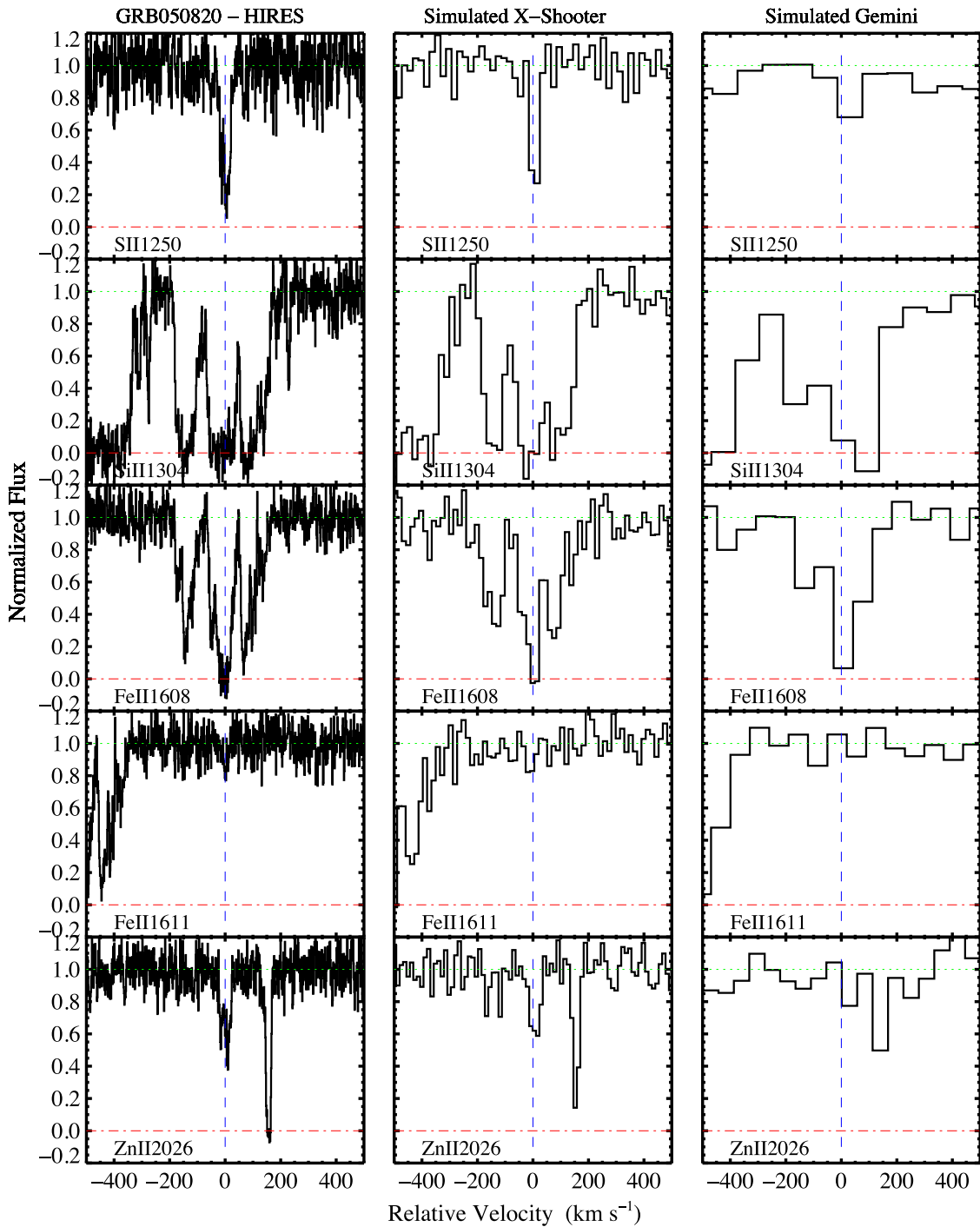


Figure 1. Left column shows weak metal lines identified in the Keck/HIRES ($R = 30,000$) spectrum of GRB 050820A, which has a true metallicity of $Z/Z_{\odot} = +0.17$. Center and right columns show the same lines resampled at the typical X-Shooter ($R \sim 6000$ in this case) and Gemini ($R \sim 1200$) resolutions, respectively, assuming an S/N = 10. The green line represents the continuum level. In case of metal-rich systems, like this example, reliable abundances can still be derived from the X-Shooter data, though blending can be an issue, while only limits can be placed from the Gemini data. Lower resolution instruments are even more heavily affected, making it almost impossible to determine meaningful limits on the metal abundances.

intervening systems, may occur in lower resolution spectra (this also makes the determination of the continuum level difficult and even more so with low S/N data); (2) hidden saturated lines in low-resolution spectra may not be clearly identified and thereby yield a lower value than the true abundance; (3) strong absorption features associated with moderately metal-rich systems are still detected at $R \sim 1200$ (or 200 km s^{-1} , GMOS typical resolution), but they completely

disappear or are difficult to distinguish at even lower resolution, providing uninteresting metallicity abundance limits.

In the first case, the result is an overestimation of metal abundances and de-blending procedures may be very complex, especially when trying to assess further hidden saturation of the blended components. In the second, instead, the column density is underestimated. We therefore opted to use isolated

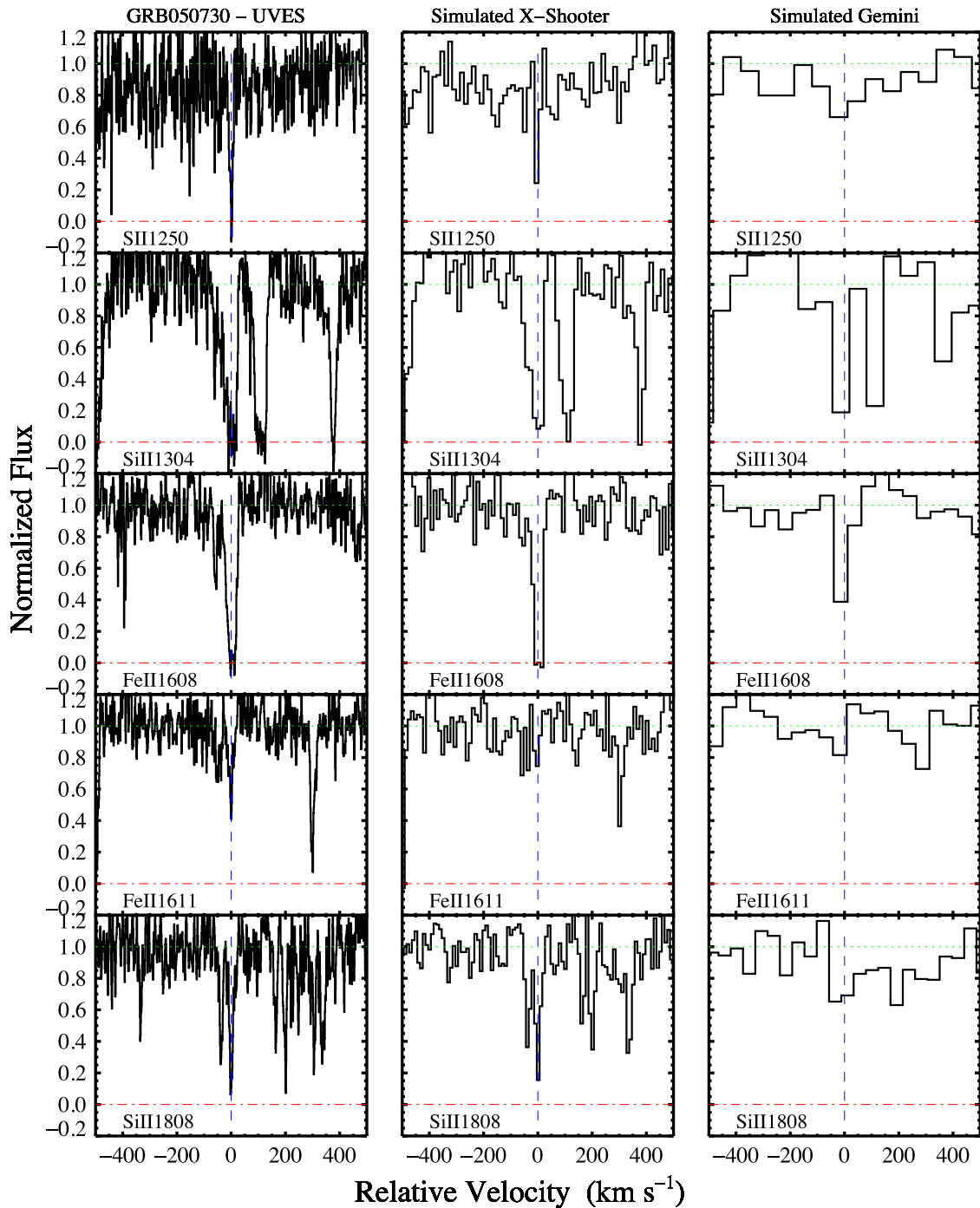


Figure 2. Same as Figure 1, this time for one of the lowest metallicity systems GRB 050730 (obtained with the VLT/UVES spectrograph, $R \sim 40,000$) which has a true metallicity of $Z/Z_{\odot} = +0.01$. In this case it is obvious that the typical lines used for metal abundance measurements are also very narrow and almost disappear even at the X-Shooter resolution. This plot shows that measuring metallicity of the order of $Z/Z_{\odot} = +0.01$ or less is very difficult and often only limits can be placed (e.g., S II 1250 or Fe II 1611).

weak lines (e.g., Fe II 1608) or very strong transitions (e.g., Si II 1526) which are likely saturated and therefore provide reasonable lower limits. In the third case it is impossible to distinguish between a true low-metallicity system and the effect of low-resolution instrumentation.

Since the majority of our spectra (34 over 55) have been obtained with $R \lesssim 2400$ and the remaining spectra with $R \gtrsim 6000$ we adopt the latter as the minimum resolution for which we can derive accurate metallicity estimates. Therefore, for all spectra with resolution lower than the X-Shooter

spectrograph (typically $R \lesssim 6000$) and $S/N > 3$, we measured metallicity from strong lines and provided only lower limits for the ionic abundances. We note that this analysis is similar to Jorgenson et al. (2013), where ionic abundances from an even lower resolution instrument, like the MagE spectrograph on the *Magellan* telescope ($R \approx 4200$), were compared with the X-shooter, UVES, and HIRES instruments. Also, while “hidden” saturation can still be present, we carefully choose features with depths that can minimize this effect (Prochaska & Wolfe 1996; Penprase et al. 2010): typically with normalized flux values

$F_\lambda < 0.5$ in any pixel in the line profile. Jorgenson et al. (2013) have also performed several simulations on the reliability of using the Apparent Optical Depth method technique in deriving ionic abundances in such spectra (AOD; Savage & Sembach 1991) in comparison with the Voigt profile fitting procedure. In order to further check this consistency we also performed a Voigt profile fitting for several ions in our X-Shooter and UVES spectra and compare these values with the ones obtained by our AOD analysis. The column densities agree with each other on average within one standard deviation. For these reasons (agreement between the AOD and Voigt profile methods, the fact that the majority of our spectra have $R \lesssim 6000$, and that our comparison sample of QSO-DLA metal abundances are also obtained with the AOD technique), we present our metallicity measurements derived with the AOD methodology in Table 1.

3.2. Neutral Hydrogen

For all the GRBs in Table 1 for which we were able to retrieve the afterglow spectra, we determine the redshift of the GRB-DLA based on the simultaneous identification of the strong Ly α feature (identifiable also at low resolution) and at least one of the fine-structure transitions (like Fe II* and Ni II*) often present in GRB afterglow spectra (Prochaska et al. 2006, 2007; Vreeswijk et al. 2007). For those cases in which fine-structure lines were not observed, e.g., due to spectral coverage, we required that at least other low ions transitions were detected at the same redshift as Ly α , or that the end of the Ly α forest was also identified.

We fit the Ly α profile with a Voigt profile using the `x_fitdla` procedure within the XIDL⁹ package, while we adopted the measurements derived in the literature if the spectra were not available (see notes in Table 1).

The QSO-DLAs measurements were obtained directly from R12 and R14, who performed a similar analysis on a sample of QSO spectra obtained with high-resolution spectrographs on the Keck telescope (e.g., HIRES or ESI).

In Figure 3 we present the column density distribution ($f_{\text{H I}}(N_{\text{H I}})$) of our two samples in comparison with the model by Noterdaeme et al. (2009; see also Wolfe et al. 1995; Péroux et al. 2003; Prochaska & Wolfe 2009; Noterdaeme et al. 2012b). As previously noted (Reichart & Price 2002; Savaglio et al. 2003; Jakobsson et al. 2006; Prochaska et al. 2007), H I column density in QSO-DLAs is a factor of ten lower than the GRB-DLAs (although see Noterdaeme et al. 2012a, 2014). This suggests that GRB-DLAs may trace a denser ISM phase, more similar to the sites of ongoing star formation (Fynbo et al. 2008b), while QSO-DLAs may probe, instead, a lower column density medium, possibly farther from dense molecular regions. Moreover, a handful of GRBs with a large amount of neutral hydrogen ($N_{\text{H I}} \gtrsim 10^{21.5} \text{ cm}^{-2}$) along their LOSs exhibit the presence of molecular hydrogen (H₂; Prochaska et al. 2009; Krühler et al. 2013; D’Elia et al. 2014), while only a few cases have been found along quasars (Noterdaeme et al. 2008; Srianand et al. 2012; Jorgenson et al. 2013, 2014).

3.3. Metallicity

Measuring the gas metal content in GRB-DLA systems is not simple, especially because some of the metals might be locked in dust grains (dust depletion effect; Savaglio et al. 2003). For example, the mildly refractory element silicon is usually depleted in the Galaxy but only marginally in DLAs and therefore it can often be used to determine the gas metallicity (Wolfe et al. 2005; Rafelski et al. 2012), assuming that this also applies to GRB-DLAs. Other good metallicity tracers include sulfur and zinc. Zinc, in particular, is often preferred because it is undepleted in the ISM and has two strong transitions at rest-frame 2026 and 2063 Å. However, it is only a trace element and therefore represents a small fraction of the mass density of the heavy element. Moreover, the evolution of zinc resembles iron only for specific star formation histories and careful modeling of zinc production by SN II and SN Ia shows an underproduction of Zn and Mg compared to S, invoking additional production sites, such as intermediate-mass stars, in order to reconcile their abundance values (see Fenner et al. 2004 for a detailed description). Therefore, as pointed out by Rafelski et al. (2012) and Prochaska (2006) we decided to use low-ionized transitions of sulfur (e.g., S II 1250), silicon (e.g., Si II 1808), and iron (e.g., Fe II 1611), in order of importance. We only use the zinc lines in the few cases where the previously discussed lines are unavailable, such as when they fall at the location of atmospheric telluric bands.

We measured ionic abundances using the Apparent Optical Depth method (Savage & Sembach 1991), which relies on the identification of several unsaturated lines of the same species and provides accurate measurements with no assumptions on the features of the Doppler parameter as other methods (like COG analyses, Carroll & Ostlie 1996). As we mentioned earlier these values agree well with the Voigt profile fitting technique.

In some cases, due to the presence of saturated transition, we only estimate lower limits on the overall metallicity (see also Savaglio & Fall 2004; Prochaska 2006; Savaglio 2006). In fact, to be conservative we consider all our measurements from low-resolution data as lower limits.

In Table 1 we summarize our findings, including H I and metallicity measurements, such as $[X/H]$ relative to solar¹⁰, and the ion used along that specific LOS. No dust depletion or ionization correction has been applied (see Sections 4.3 and 4.2). In the last column we list the references relative to each GRB and, in the Appendix, we briefly describe each LOS in more detail.

4. DISCUSSION

4.1. Possible Observational Biases

First of all we need to understand if there are possible biases that might affect either sample: GRBs are selected solely on the prompt emission detection in the gamma-ray energy bands from dedicated satellites (e.g., *Swift*). The spectra were taken mostly independently of the brightness of the afterglow, although a preference in observing brighter events might be present. Neither of these two selection criteria (brightness in the gamma-ray bands or in the optical) seem to explain the difference in $N_{\text{H I}}$ distribution (Figure 3). As previously noted by Pontzen et al. (2010), GRB-DLAs seem to probe a type of

⁹ <http://ucolick.org/~xavier/IDL>

¹⁰ $[X/H] = \log[X/H]_{\text{DLA}} - \log[X/H]_{\odot}$.

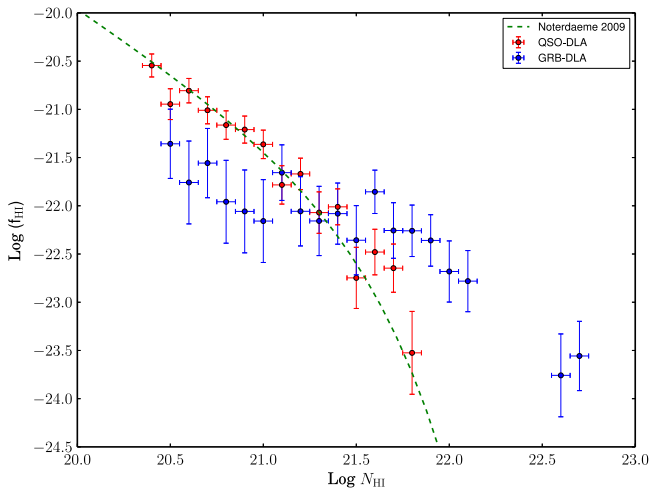


Figure 3. Column density distribution for our two DLA samples (QSO in red and GRB in blue). Vertical error bars are derived assuming Poissonian distribution (95% confidence level) and we overplot in green (dashed line) the model by Noterdaeme et al. (2009). Despite the fact that the GRB-DLA sample is a factor of four smaller, there is a clear overlap in the distribution around $N_{\text{HI}} = 21.5$, while GRB-DLAs show a much larger number of dense systems compared with the QSO-DLA sample (see also Noterdaeme et al. 2014, indicating that GRBs are located, if not embedded, in very dense regions within their host galaxies, that can be the beacons of present star formation.

absorber different from the QSO-DLA population. In particular, if the faint afterglows were not observed spectroscopically because of some high level of extinction (like the “dark” GRBs from Perley et al. 2013), and assuming a possible correlation between metallicity and visual extinction (see Zafar & Watson 2013), this would bias us toward lower metallicities. This, combined with a small number of metal-poor GRB-DLAs at high- z suggests that, if such a bias exists, it would have a small effect, also because at high redshift there are fewer dusty systems (Covino et al. 2013). At $z \gtrsim 6$, our understanding of dust production mechanisms (e.g., SN, AGB stars) are still to be fully understood, although some advancements have been made both theoretically and observationally (Gall et al. 2011). We also note that, similarly to these authors, we are assuming the extinction along the LOS to be the same as the one derived from afterglow studies, which in principle can lead to different estimates with respect to the host galaxy extinction (see Elliott et al. 2013; Perley et al. 2013, for a comparison between the afterglow- and host-derived extinction). Overall, despite the large sample presented here, our conclusions, in particular at high redshift, require more data in order to better assess the effect of such observational biases.

The QSO sample from R12 and R14, instead, has been selected solely on the presence of a $\text{Ly}\alpha$ line in their SDSS spectrum and $\log N_{\text{HI}} \geq 20.3$, and therefore represents an unbiased sample with respect to the gas metallicity (Rafelski et al. 2012). The $z \lesssim 2$ QSO-DLAs were selected based on the presence of Mg II in the SDSS spectra, implying a small bias against low-metallicity systems at such redshift. Since our redshift range of interest is mostly at $z \gtrsim 2$, this should not be a source of significant concern.

4.2. Ionization Correction

The identification of fine-structure transitions and the line profile variability within the first hour after the GRB explosion have been associated with the effect of an evolving radiation

field from the GRB (like the afterglow) or nearby young stars onto the progenitor’s surrounding medium (Prochaska et al. 2006; Vreeswijk et al. 2007; de Cia et al. 2012). This process directly affects metal abundance measurements and the inferred metallicity ionization correction is strongly dependent on the hydrogen column density (Vreeswijk et al. 2013).

Distinguishing between ionized (photoionized or excited) gas from the GRB emission in the vicinity of the GRB progenitor and the bulk of the host galaxy ISM, which is also ionized by the surrounding radiation field, is a complicated process: if the gas probed by the afterglow spectroscopy is close to the GRB ($\lesssim 200$ pc), then the ionization is increasing with time and complex modeling is required to estimate the time-dependent ionization correction (Krongold & Prochaska 2013). The most important example in which a detailed photoionization modeling (including photo-ionization and excitation effects) has been performed is probably the sub-DLAs GRB 080310 (Vreeswijk et al. 2013). In most of our GRB-DLAs, the data have been acquired at much later time and in several cases, when multiple spectra were obtained, these objects do not present line profile variation: such non-variability suggests that we are likely probing the ISM at larger distances and/or gas clouds unaffected by the GRB radiation.

Reassuringly, models similar to the ones of Vreeswijk et al. (2013) have been used in GRB-DLA spectra (Ledoux et al. 2009): ionization corrections are often minimal ($\lesssim 10\%$) compared to other even extreme cases, e.g., star-forming galaxies or $\text{Ly}\alpha$ emitters. For these reasons we did not apply any ionization correction to our derived column densities and our final metallicity measurements. We stress that the ionization correction is an important aspect of the column density determination and requires particular attention and a much larger sample of rapid high-resolution spectroscopic observation sequences starting not later than a few minutes after the burst. While this is the least known quantity in our study, we argue that our results are indicative of an overall general characterization of the GRB-DLA population. A large sample of multi-epoch high-resolution data sets and accurate modeling are still needed, but these are beyond the scope of this paper.

4.3. Depletion Correction

Understanding the effect of dust depletion in DLAs requires the determination of ionic abundances of both refractory and non-refractory elements (see for example D’Elia et al. 2014). Savaglio & Fall (2004) determined for the first time such “depletion pattern,” while recently de Cia et al. (2013) compared a sample of 20 GRB-DLAs with 47 QSO-DLAs in order to study the dust-to-metal ratio of these systems. These authors used $[\text{Fe}/\text{Zn}]$ as dust indicator and found that the dust depletion correction is in the most depleted cases $\sim +0.1$ dex, independent of metallicity.

These results are in contrast to those of R12, where strong iron depletion is present at $Z/Z_{\odot} > -1.0$. Instead, R12 shows that silicon is rarely depleted in QSO-DLAs and that depletion effects are relevant only at high metallicity ($\gtrsim -0.3 Z/Z_{\odot}$), and therefore are minimal for the majority of our GRB LOSs (see also Vladilo et al. 2011).

For our GRB-DLA sample, calculating the depletion correction is not always possible, especially for our low resolution GRB-DLA spectra. Also, in the few cases where iron

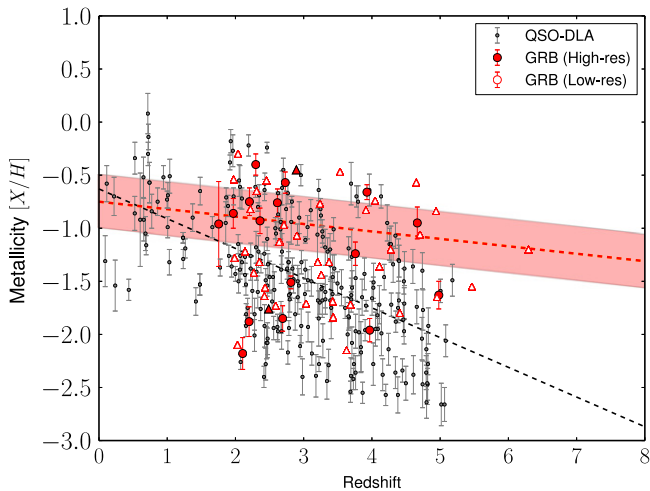


Figure 4. Metallicity evolution with redshift for the GRB (red) and QSO (gray) samples. Lower limits are indicated by upward triangles, while filled/open symbols indicate if these values come from high/low resolving power instruments. We perform a linear regression fit of the GRB-DLA data using the Schmitt survival analysis method, which takes into account the censoring within the data set (red dashed line). The shaded area represents the 1σ error in the fitting parameters obtained using 500 bootstrap iterations. A linear fit of the QSO-DLA metallicity is marked by the dashed black line (see the text for details). The GRB sample, despite the large scatter in $[X/H]$, seems to probe an environment which slowly declines across the $z = 1.8\text{--}6$ redshift range.

was used, we derived $Z/Z_{\odot} < -1.0$, so depletion correction should be minimal.

Nevertheless, the application of a depletion correction would increase the metallicity of our systems, strengthening some of our conclusions (see Section 5). Therefore, we choose not to apply any depletion correction to the measured metallicities. Finally, we performed α -enhancement correction to the iron-based metallicities for our high-resolution sample using the correction factors adopted by R12.

4.4. Metallicity Evolution

Our findings are shown in Figure 4, where the QSO-DLA (in gray) and GRB-DLA (in red) metallicities are plotted. We perform a linear fit of the metallicity measurements (and limits) with redshift using a survival analysis technique (Schmitt 1985), which takes into account upper and lower limits. In particular we used the `statistics.schmittbin` package within the IRAF¹¹ distribution. We also used bootstrap sampling to determine the 1σ error in the fit (with 500 iterations).

Ideally, we would like to use our metallicity measurements to investigate the cosmic metal budget at different epochs: this is usually done by weighting the average metallicity over a specific redshift bin with the total neutral hydrogen column density in the same redshift interval (see R12 and R14 for the QSO-DLA sample). Unfortunately, because the large number of limits present in the GRB-DLA sample we simply fit the metallicity of the single systems, which still provides useful insight into the DLA populations' metal content.

For the GRB-DLA sample, we derive $[X/H]_{\text{GRB}} = (-0.07 \pm 0.06)z - (0.75 \pm 0.25)$ (thick red dashed line), which is also consistent with no evolution (at the

1σ confidence level). For the QSO-DLA sample we derive a linear trend between redshift and DLA metallicity, which is given by $[X/H] = (-0.20 \pm 0.03)z - (0.68 \pm 0.09)$ (thick black dashed line in Figure 4).

To test the reliability of our fit and sensitive this is to the small number of abundance measurements (while respecting the limits) we ran a series of Monte Carlo simulations: we created 1000 mock samples of GRB-DLA metallicity measurements and limits (with values within the typical GRB-DLA high-resolution points rms) and we repeated the survival analysis fit. Assuming an intrinsic true slope from the QSO-DLA distribution of -0.2 we obtained a slope > -0.07 or less only in 7% of the cases, which means that it is unlikely that our results are affected by low number statistics. Similar tests with different intrinsic distribution (from flat to very steep metallicity evolution) provide similar results and reassure us that, despite the small number statistics, we can recover the input slopes to within the reported 1σ confidence interval.

Finally, we point out that GRB-DLAs and QSO-DLAs have a similar metallicity distribution at $z \sim 2\text{--}3$, suggesting that there is no difference between the two populations of absorbers in terms of metal content. We performed a two-sample Kolmogorov–Smirnov test between these subsamples using the IRAF `stdas.analysis.statistics.twosamp` task and we can rule out the null hypothesis that the two distributions are drawn from the same parent population at the 90% confidence level. Instead, if we naively consider the lower limits as actual measurements and apply an arbitrary correction of different values (from $+0.1$ to $+0.3$ dex), there remains evidence that the two distributions are distinct even when the highest value is considered ($+0.3$ dex), but the statistical significance is $< 99\%$.

However, the GRB-DLA metallicity declines suggests that, in particular at $z \gtrsim 3$, the GRB-DLA environment is more metal-enriched than in QSO-DLAs, likely by active star formation episodes. These metals may have been ejected by SN explosions or mass losses and polluted the GRB progenitor's neighborhood before the GRB occurred (Matteucci & Recchi 2001; Kröger et al. 2006; Mao 2010; Kulkarni et al. 2013). If this is true, the inferred metallicity may not reflect the overall metal content of such high- z GRB host galaxies, although we know that the gas intercepted by GRB afterglow spectra may lie up to a few kpc from the GRB explosion site (see the next section).

4.5. Characterizing these DLA populations

We will now try to understand the difference in the metallicity evolution between the GRB- and QSO-DLA samples. For example, if GRB-DLAs trace the general host galaxy ISM, this gas ionization state may show the effect of whatever local ionization field is in the vicinity of the GRB or along the LOS.

Prochaska et al. (2007) argued that the size of such a molecular cloud would exceed the largest molecular cloud in the local group, so the GRB-DLAs are tracing material as far as at least 100pc from the GRB (and even out to ≈ 2 kpc in the case of GRB 060418; Vreeswijk et al. 2007). The fact that in the $z = 3.5\text{--}6$ redshift range the metallicity of the gas is, on average, 10% of the solar value suggests that a substantial amount of metals is already present at high redshift.

These estimates are in agreement with the most recent GRB progenitor models (Woosley 2011; Woosley & Heger 2012): if

¹¹ IRAF is distributed by the National Optical Astronomy Observatory, which is operated by the Association of Universities for Research in Astronomy under cooperative agreement with the National Science Foundation.

the GRB host galaxy is metal-rich, then a large amount of metals have been produced by SNe or, in the highest redshift bin observed, by a late population of PopIII stars (or more likely early PopII). Nevertheless, in order to be able to produce a GRB explosion from Wolf–Rayet type stars, the amount of metal injected into the ISM and mixed throughout the host galaxy has to be below a certain threshold to retain enough angular momentum and minimize the stellar mass loss of the progenitor (Woosley & Heger 2006; Woosley 2011; Woosley & Heger 2012). Clearly more data need to be acquired, in particular at high- z , to confirm the existence of such limits, and also in light of the high-metallicity hosts observed (e.g., Krühler et al. 2012; Savaglio 2012; Elliott et al. 2013).

On the other hand, DLAs identified in QSO spectra are cross-section dependent, and therefore they might not trace the denser part of the galaxies (as for GRB-DLAs). Also, it has been proposed that a combined large sample of GRB- and QSO-DLAs may represent a complete census of $z \approx 3$ star-forming galaxies that could be missed by magnitude limited surveys (Fynbo et al. 2008b).

Finally, as R14 pointed out, the observed metallicity decrement at $z \gtrsim 4.7$ suggests an increase in the covering fraction of neutral gas: similar behavior in fact can be produced by the combination of increased density of the universe and lower background radiation field, which allows the hydrogen gas to be self-shielded at the lower density as a function of redshift (Fumagalli et al. 2013). In this picture, the denser region would reside in the halo of the galaxies or in the IGM where the star formation, and therefore metal enrichment, is lower.

4.6. GRB-DLA metallicity in context

A long-standing debate exists as to the degree to which GRBs faithfully trace the cosmic star formation rate. Although GRBs have been associated with broad-lined SNe at low redshift and regions of active star formation in their host galaxies, spectroscopic observations have shown that GRB host galaxies tend to be relatively metal-poor compared to SNe Ibc hosts (Modjaz et al. 2008). This observed preference for low metallicity environments may impart a redshift dependent bias in the type of star-forming regions that can produce a GRB (Kocevski et al. 2009; Trenti et al. 2014).

In particular, at low redshifts ($z \lesssim 1$), a preference for low metallicity environments would limit GRBs to low mass spirals and dwarf galaxies (e.g., Levesque et al. 2010), due to the well established relationship between mass and metallicity (see Kocevski & West 2011; Graham & Fruchter 2013, and references therein). At higher redshifts, the mass range of galaxies capable of hosting a GRB would increase to include more massive, star-forming galaxies, since the average metallicity of all galaxies in the universe falls. Recent unbiased searches of GRB host galaxies like the *TOUGH* survey (Hjorth et al. 2012) or of the host galaxies of the “dark” GRB population (Perley et al. 2013) largely support this trend. These surveys find that bursts at intermediate redshifts tend to be drawn from star-forming galaxies with a greater diversity of mass, morphology, and dust content, suggesting that high redshift GRBs may serve as more faithful tracers of cosmic star formation compared to their low redshift counterparts (see also Hunt et al. 2014; Perley et al. 2014).

Our sample of GRB-DLAs, although not a complete host sample, covers a much greater redshift range than the emission-

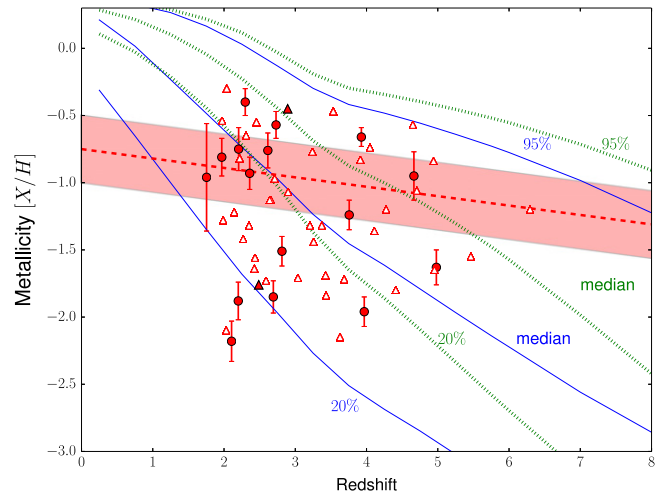


Figure 5. Adapted from Trenti et al. (2014). The colored lines represent two particular models for GRB hosts metallicity assuming a mild metallicity bias ($p = 0.04$, solid blue) and no bias at all (dotted green). Lines also indicate the trends for the top 95%, the median, and lower 20% of the simulated GRB host population. The mild bias model is broadly capable of reproducing the observed metallicity distribution of our biased sample of GRB-DLAs at a specific redshift, while the “no bias” is largely inconsistent with the data.

line-derived measurements in these studies and, more importantly, does not depend on strong observational biases (e.g., brightness of the host, intensity of the emission lines), although we may miss some dusty (therefore metal-rich) events. Based on the arguments outlined above, even as metallicity-biased tracers of star formation, the GRB-DLA results presented in Figure 4 should become more representative of the metallicity evolution of the general star-forming galaxy population with increasing redshift. However, a better understanding of both observational biases (Fynbo et al. 2008a, 2008b) and the effect of metallicity in GRB production (Jakobsson et al. 2013) is required before we can fully address the connection between the environments that are capable of producing GRBs and the conditions of star-forming regions in the early universe.

From a theoretical standpoint, recent simulations by Trenti et al. (2014) have been suggesting that two combined channels of GRB populations exist: one, the “collapsar” mode, which strictly depends on the host metallicity, and a second one, the “binary stars” mode, which is metallicity independent. Assuming these two modes coexist and the mass–metallicity relation of star-forming galaxies is known, these authors predict the GRB host galaxy metallicity redshift evolution with different combinations of these two channels (from strong metallicity bias to an almost negligible one). Unfortunately, metallicity measurements from emission line diagnostics are not yet available for $z \gtrsim 1$ host galaxies, but our sample represents the best opportunity to test these models.

In Figure 5 we present our metallicity results in comparison the predicted metallicity for the upper 95%, the median, and the bottom 20% of the GRB host galaxies distribution, assuming an absent (dotted lines) and a moderate (solid lines) metallicity bias (adapted from Trenti et al. 2014, using a value of $p = 0.04$).

These models essentially predict that in any given redshift bin, for example, 20% of the hosts that produce a GRB have metallicity below the lower solid line. Indeed, focusing on the redshift $z = 2$ -3 range, 5 out of 27 hosts have metallicity below the line. On the other hand the “no-metallicity bias” model does

not agree with the data. Overall, it seems that at least at $z \lesssim 4$ a moderate metallicity bias is required in order to reconcile theory and observations (Vergani et al. 2014), although a more detailed analysis of these models and the implications on the metallicity cut-off in the GRB host masses is needed, in particular to understand the role of such metallicity bias, if it indeed exists, at higher redshift.

5. CONCLUSIONS

In this work we investigated the properties of GRB LOSs that show evidence for DLAs within the GRB host galaxy. Similar systems have been studied along QSOs in order to understand the chemical enrichment and the metal evolution in cold gas systems over cosmic times.

We collected all the publicly available GRB afterglow spectra, including data already published in the literature and we uniformly analyzed these LOSs in order to obtain metal abundances using mildly or non refractory species (e.g., sulfur, silicon, and zinc). In particular, we opted for a conservative approach when considering low-resolution data (see Section 3.1): we consider depletion correction to our metal abundance measurements to have a negligible effect (see Section 4.3). Also, we note that ionization correction may have an important role in estimates derived from very early time spectroscopic data ($\lesssim 10$ minutes) due to the highly variable ionization flux from the GRB itself. Nevertheless, since most of our data have been acquired at much later times and the fact that detailed analyses are not always possible (especially with low-resolution data) we do not consider such a correction in our analysis (see Section 4.2).

In Figure 4 we present our GRB-DLA metallicity evolution fit in comparison with the QSO-DLA results from R12. We performed a detailed survival analysis fit to accurately take into account all the limits present in our data set. As in previous works (Savaglio 2012; Arabsalmani et al. 2015) we derive a much shallower decline of the GRB host metallicity with redshift relative to the QSO-DLA sample suggesting a somewhat metal-rich environment for the GRB host galaxies (in particular at $z > 4$), but still below solar values, in agreement with GRB progenitor models (Woosley & Heger 2012). At $z \lesssim 3$ there is a reasonable overlap between the two populations, according to their metallicity properties, indicating similarities between the two DLA populations, despite the higher H I column density traced by the GRB-DLAs. At higher redshift, GRB-DLAs seem to prefer higher metallicities than QSO-DLAs. Despite the small number of high-resolution data, a few LOSs (e.g., GRB130606A or GRB060510B) seem to indicate that these GRB-DLAs point toward a denser, metal-richer environment, likely tracing a less common population of metal-rich DLAs.

Overall, our findings confirm the idea that moving toward higher redshifts, GRBs preferentially trace a denser metal-rich environment within galaxies, while the QSO-DLA population may be progressively dominated by neutral regions with minor star formation. In other words, the absence of metal-poor ($[X/H]_{\text{GRB}} \lesssim -1.5$) GRB-DLAs at high- z seems to indicate that such GRB-DLA hosts are at the low-end of the luminosity (or mass) distribution and do not present high star formation (and GRB progenitors). Another possibility is that these GRBs occurred in completely different environments (galactic halos). Deep imaging, with 8–10 m telescopes or with *HST* is needed in order to fully characterize these hosts.

Finally, we compare our findings with the most recent model prediction of GRB host galaxy metallicities (Figure 5, Trenti et al. 2014). Our results broadly agree with host galaxy metallicity predictions where two-channels for GRB productions are considered (collapsars and binary) and mildly affected by a metallicity bias. The model predicts well the metallicity distribution for the bottom 20% and median of the host population, though more work is required to fully understand this metallicity bias and its effect on other properties of the GRB host population (e.g., the host mass limit driven by a metallicity cut-off; Kocevski et al. 2009).

Our GRB-DLA host galaxies represent the largest sample available to date and, although not complete, it is suitable for multi-band follow-up, in particular for the current and upcoming near-infrared spectroscopic instruments, which will allow us to determine the SFR and metallicities directly using emission line diagnostics. Also, determining the hosts' properties, like mass and rest-frame UV star formation, will help in better characterizing the overall high- z GRB host population, and their capability to harbor GRB progenitors. Furthermore, we will be able to better understand the observational biases that might affect our results, especially at high- z , where few LOSs are observed (including dust extinction and/or cosmic metallicity trend).

While multiband surveys of this sample of GRB-DLA hosts will allow a better characterization of these galaxies, the advent of future missions like the *James Webb Space Telescope* and the new generation of 30 m telescopes will be able to identify these faint hosts at the highest redshifts and spatially resolve the regions of star formation traced by GRB-DLAs, which seem to hide the secrets of primordial star formation sites.

This research was supported by the NASA Postdoctoral Program at the Goddard Space Flight Center, administered by Oak Ridge Associated Universities through a contract with NASA. A.C. thanks M.F. and M.R. for the incredible support and useful discussions during the writing of this work. A.C. also thanks M.T. for fundamental discussion as well for providing the models' curves. M.F. acknowledges support by the Science and Technology Facilities Council (Grant #ST/L00075X/1). A.C. thanks P. D'Avanzo for providing the spectrum of GRB 090205A.

APPENDIX DESCRIPTION OF RELEVANT SPECTRA

A.1 GRB000926

Our results confirm the findings published in the literature. The low-resolution data however only allows a lower limit based on the Zn II lines to be placed (also consistent with Prochaska 2006).

A.2 GRB011211

Our examination of the FORS spectrum allows a lower limit based on the Si II line of $[X/H] \gtrsim -1.22$ to be placed, consistent with the result of Prochaska (2006).

A.3 GRB020124

We derived a $N_{\text{H I}}$ value similar to that in the work of Hjorth et al. (2003a), but the spectrum has S/N too low to provide an adequate metallicity measurement.

A.4 GRB021004

Extensive literature is present for this GRB sub-DLA (e.g., Fiore et al. 2005; Fynbo et al. 2005; Lazzati et al. 2006; Castro-Tirado et al. 2010). We report this GRB here for completeness.

A.5 GRB030226

We also notice the presence of an intervening system along this sightline at $z_{\text{int}} = 1.96236$. Based on some isolated Iron lines we place a lower limit on this GRB-DLA consistent with the measurement of Shin et al. (2006). Our iron-derived metallicity limit is also consistent with the measurement reported by Schady et al. (2011), considering the large uncertainty in the H I estimate (0.3 dex).

A.6 GRB030323

Our analysis is consistent with the previous work by Vreeswijk et al. (2004; including the difference in the sulfur solar abundance between Grevesse & Sauval 1998 and Asplund et al. 2009) and Prochaska (2006).

A.7 GRB030429

The spectra has been presented before by Jakobsson et al. (2004). The lower limit in the metallicity is given by the few detected lines (e.g., Si II).

A.8 GRB050319

The spectrum has been presented in Fynbo et al. (2009); we adopt the measurement from Laskar et al. (2011) as an upper limit based on Si II 1526.

A.9 GRB050401

The spectrum was presented by Watson et al. (2006). We obtain similar results and adopt a value of $[X/H] \gtrsim -1.07$ based on the Zn II line measurement.

A.10 GRB050505

The metallicity we derived from sulfur measurements is similar to what has been presented by Berger et al. (2006), though we consider this to be a lower limit.

A.11 GRB050730

The high resolution allows an accurate determination of metallicity using different tracers. Our results presented in Table 1 are consistent with the published values of D'Elia et al. (2007) and Prochaska et al. (2008).

A.12 GRB050820

The measurement we obtained based on sulfur lines is consistent with the results from Jakobsson et al. (2006) and Prochaska et al. (2007).

A.13 GRB050904

As noted by Thöne et al. (2013), the values reported in the literature (Kawai et al. 2006) are likely an overestimation due to the blending of different lines, so we adopt their sulfur measurement, $[S/H] \gtrsim -1.0$, as a lower limit for this GRB.

A.14 GRB050908

This is a sub-DLA system, so it is included for completeness.

A.15 GRB050922C

The values reported by Fox et al. (2008) and Prochaska et al. (2007) are consistent with our own measurement.

A.16 GRB051111

Only an upper limit has been derived for this GRB.

A.17 GRB060115

These dates are part of the compilation from Fynbo et al. (2009). Our estimated lower limit is mostly based on S II lines.

A.18 GRB060124

This is a sub-DLA system, so it is included for completeness.

A.19 GRB060206

Our analysis is consistent with the results of Fynbo et al. (2006), but we consider our estimated value of $[X/H] = -0.74$ a lower limit, based on the strength of the same sulfur lines.

A.20 GRB060210

This GRB spectrum shows the presence of a nearby intervening systems at $z_{\text{int}} = 3.817$. Despite its presence, a stringent lower limit of $[X/H] \gtrsim -0.83$ can be placed based on iron and silicon lines.

A.21 GRB060223

The value from Chary et al. (2007) has been adopted.

A.22 GRB060510B

We confirm the result from the literature based on sulfur lines (Chary et al. 2007; Price et al. 2007).

A.23 GRB060522

The value of $N_{\text{H I}}$ from Chary et al. (2007) has been adopted, but there are no metal lines detected.

A.24 GRB060526

This is a sub-DLA system, and so is included for completeness.

A.25 GRB060605

This is a sub-DLA system, and so is included for completeness.

A.26 GRB060607A

This is a sub-DLA system, and so is included for completeness.

A.27 GRB060707

We confirm the analysis of Jakobsson et al. (2006), but the low-resolution data only allows a conservative lower limit of $[X/H] \gtrsim -1.69$, based on weak Fe II transitions, to be placed.

A.28 GRB060714

The spectrum has a higher S/N and similar to GRB060707 we could derive a lower limit, but in this case we used Zn II lines (Jakobsson et al. 2006).

A.29 GRB060906

This spectrum was presented by Jakobsson et al. (2006) and metallicity measurements were recently presented by Laskar et al. (2011). Using sulfur lines we derive $[X/H] \geq -1.72$.

A.30 GRB060926

For this GRB we used likely saturated Zn II lines and place a lower limit of $[X/H] \geq -1.32$.

A.31 GRB060927

This low S/N spectrum has been published before (Ruiz-Velasco et al. 2007). We derived more stringent limit than the ones derived by Laskar et al. (2011) using S II saturated lines.

A.32 GRB061110B

This spectrum is part of the compilation of Fynbo et al. (2009). We obtained a measurement similar to Laskar et al. (2011), but we consider this a lower limit.

A.33 GRB070110

This spectrum is part of the compilation of Fynbo et al. (2009); we performed our own metallicity measurement.

A.34 GRB070411

This is a sub-DLA system, and so is included for completeness.

A.35 GRB070506

This spectrum is part of the compilation of Fynbo et al. (2009). We also identified an intervening system at $z = 2.071$. We derived a metallicity lower limit for the host from Zn II lines.

A.36 GRB070721B

This spectrum is part of the compilation of Fynbo et al. (2009). The low resolution of this spectrum allows only a lower limit estimate from Si II.

A.37 GRB070802

This spectrum is part of the compilation of Fynbo et al. (2009) and has been studied by Elíasdóttir et al. (2009). The low-resolution of this spectrum only allows a lower limit estimate from blended Si II: we are a bit more conservative than the previous work by Elíasdóttir et al. (2009), but the two values are within 0.1 dex, which is below the typical uncertainty for these low-resolution data sets.

A.38 GRB071020

This GRB is likely a sub-DLA system, and so is included for completeness.

A.39 GRB071031

This spectrum was presented by Ledoux et al. (2009). Most of the useful metal lines are saturated (e.g., S II 1259). Using weak Fe II features (e.g., Fe II 1611) we obtained similar results $[X/H] = -1.85 \pm 0.12$ (see also Fox et al. 2008).

A.40 GRB080210

This GRB was observed with the FORS2 instrument at several different resolutions (see de Cia et al. 2011). Our results, based on our analysis of the same FORS2 data, show similar results, though we consider these metallicity estimates a lower limit (see Section 3.1).

A.41 GRB080310

This GRB is likely a sub-DLA system, and so is included for completeness.

A.42 GRB080413A

This spectrum was presented by Fynbo et al. (2009) and the metallicity was estimated by Ledoux et al. (2009). We only derived a lower limit based on zinc and nickel lines, which are also consistent with these previous works.

A.43 GRB080607

This GRB spectrum was presented by Prochaska et al. (2009) and it shows for the first time the clear presence of H₂ molecular lines in a GRB afterglow spectrum. Using different metallicity tracers, we retrieve similar values for the metallicity limits ($[X/H] \geq -1.71$).

A.44 GRB080721

This spectrum was presented by Starling et al. (2009). We derived a more conservative lower limit, using multiple α -elements lines.

A.45 GRB080804

The spectrum was presented by Fynbo et al. (2009). We determine the metallicity and relative depletion using iron as well as non-refractory elements.

A.46 GRB080810

This GRB is likely a sub-DLA system, and so is included for completeness.

A.47 GRB080913

This GRB is likely a sub-DLA system, and so is included for completeness.

A.48 GRB081008

This spectrum has been presented by D'Elia et al. (2011). We obtained a similar metallicity estimate. We also analyzed a Gemini/GMOS spectrum from which we derived consistent lower limits. We used our UVES spectrum measurements.

A.49 GRB090205

This LOS appears in D'Avanzo et al. (2010). In particular, we note that these authors reported sulfur column abundance

from blended profiles. We derived a similar metallicity lower limit of $[X/H] \geq -0.57$.

A.50 GRB090323

This GRB has a complex structure, with two absorbers within 600 km s^{-1} (Savaglio 2012), one of which is a sub-DLA. Due to the complexity of this LOS and the low-resolution of the VLT/FORS spectrum, we exclude GRB 090323 from our analysis. We report the metallicity in Table 1 for completeness.

A.51 GRB090426

This GRB is likely a sub-DLA system, and so is included for completeness.

A.52 GRB090516

These data were presented by de Ugarte Postigo et al. (2012), but only equivalent widths were provided. Our analysis of the low-resolution VLT/FORS2 spectrum results in a lower limit of the metallicity of $[X/H] \geq -1.36$.

A.53 GRB090809

We measured a slightly higher metallicity than the one obtained by Skúladóttir (2010): nevertheless our silicon-derived metallicity value (see Table 1) is well within 2σ from the one presented by these authors.

A.54 GRB090812

These data were presented by de Ugarte Postigo et al. (2012). We estimated a lower limit based on α -element absorption features.

A.55 GRB090926

A VLT/FORS2 spectrum was presented by Rau et al. (2010), while a series of X-Shooter spectroscopic observations was presented by D’Elia et al. (2010). We obtained similar results; in particular the X-Shooter resolution allows stronger constrain on the metallicity.

A.56 GRB100219

This spectrum was presented by Thöne et al. (2013). We supplement this data set with a Gemini/GMOS spectrum. We also reanalyzed the X-Shooter spectrum. Our measurement is slightly higher than the one presented by these authors, but within their error (0.2 dex).

A.57 GRB100425

We analyzed this data set using the phase 3 products provided by the ESO database. Our metallicity lower limit is consistent with the one derived by Skúladóttir (2010).

A.58 GRB110205

This spectrum was already presented by Cucchiara et al. (2011a).

A.59 GRB111008A

This X-Shooter spectrum was presented by Sparre et al. (2014). Our iron and sulfur metallicity estimates are consistent

with the ones presented in this work. We report the former as a metallicity tracer.

A.60 GRB111107A

This X-Shooter spectrum has not been presented in previous works. The S/N of the spectra is low, and therefore our metallicity measurement, based on saturated sulfur lines, has to be considered a lower limit.

A.61 GRB120327A

This spectrum has been published by D’Elia et al. (2014). Our sulfur measurement agrees with these authors.

A.62 GRB120716A

This spectrum has not been published in the literature before. The spectrum was obtained 2.6 days after the GRB has been discovered. Despite the low S/N we report a metallicity of $[X/H] \geq -1.76$ based on identified iron lines.

A.63 GRB120815A

This GRB spectrum has been published by Krühler et al. (2013). Our analysis is consistent with these authors’ results.

A.64 GRB120909A

This X-Shooter spectrum has not been presented before. We derive metallicity measurements from weak iron lines as well α -elements.

A.65 GRB121024A

This X-Shooter spectrum has recently been presented by Friis et al. (2014). We also identified multiple systems at $z_1 = 2.3014$ and an intervening one at $z_2 = 2.2977$ (corresponding to 400 km s^{-1}). Fine-structure transitions are identified corresponding to the z_2 system, suggesting that the cloud at z_1 is at a large distance from the GRB radiation field. The broad, saturated Ly α profiles make it hard to discern between the two components. Therefore we opted to consider them as one single absorber. The metallicity from the zinc lines is reported in Table 1, while we can infer a large depletion factor from iron lines (for a detailed analysis see Friis et al. 2014).

A.66 GRB121201A

This X-Shooter spectrum was preliminary presented in GCN only (Sanchez-Ramirez et al. 2012). This LOS present a possible Ly α emission line. Unfortunately the S/N is low ($S/N \lesssim 3$) and at the line redshift ($z = 3.385$) it is difficult to identify metal lines unambiguously. We therefore decide to report only the neutral hydrogen column density.

A.67 GRB130408A

This GRB has been observed by our team (Tanvir et al. 2013) as well as by the VLT/X-Shooter (Hjorth et al. 2013). We analyzed both spectra and report the metallicity measurements from both analyses. The X-shooter derived value is plotted in Figure 4.

A.68 GRB130505A

We present our Gemini spectrum for the first time. We identified several absorption lines, and we were able to determine a lower limit on the metallicity based on weak iron transition (Fe II 1608).

A.69 GRB130606A

This spectrum has been published by Chornock et al. (2013). The LOS presents the signature of a likely sub-DLA system, and therefore we present this value here for completeness.

A.70 GRB140226A

This spectrum was obtained with the Keck/LRIS instrument. Several metal lines have been identified, but the low resolution of this instrument allows only a metallicity lower limit from iron and sulfur lines to be placed.

A.71 GRB140311A

This spectrum was obtained by our collaboration and presents few metal absorption features. We were only able to place a lower limit on the metallicity based on nickel lines, since the sulfur lines seem contaminated by other lines.

A.72 GRB140419A

This is a sub-DLA system, and so is included for completeness.

A.73 GRB140423A

We present our analysis on our Gemini/GMOS spectrum (Tanvir et al. 2014). Based on α -elements lines and weak iron lines (e.g., Fe II 1608) we were able to place a lower limit on the metallicity.

A.74 GRB140518A

This data have not been published before, but a preliminary analysis appears in Chornock et al. (2014). Our metallicity limit comes from saturated sulfur transitions.

REFERENCES

- Arabsalmani, M., Møller, P., Fynbo, J. P. U., et al. 2015, *MNRAS*, 446, 990
 Asplund, M., Grevesse, N., Sauval, A. J., & Scott, P. 2009, *ARA&A*, 47, 481
 Barkana, R., & Loeb, A. 2001, *PhR*, 349, 125
 Berger, E., Chornock, R., Holmes, T. R., et al. 2011, *ApJ*, 743, 204
 Berger, E., Penprase, B. E., Cenko, S. B., et al. 2006, *ApJ*, 642, 979
 Bouwens, R. J., Illingworth, G. D., Oesch, P. A., et al. 2014, arXiv:1403.4295
 Bromm, V. 2013, *RPPH*, 76, 112901
 Carroll, B. W., & Ostlie, D. A. 1996, *An Introduction to Modern Astrophysics* (San Francisco, CA: Benjamin Cummings)
 Castro, S., Galama, T. J., Harrison, F. A., et al. 2003, *ApJ*, 586, 128
 Castro-Tirado, A. J., Moller, P., García-Segura, G., et al. 2010, *A&A*, 517, A61
 Cenko, S. B., Frail, D. A., Harrison, F. A., et al. 2011, *ApJ*, 732, 29
 Chary, R., Berger, E., & Cowie, L. 2007, *ApJ*, 671, 272
 Chen, H.-W., Prochaska, J. X., Ramirez-Ruiz, E., et al. 2007, *ApJ*, 663, 420
 Chen, K.-J., Bromm, V., Heger, A., Jeon, M., & Woosley, S. 2015, *ApJ*, 802, 13
 Chornock, R., Berger, E., Fox, D. B., et al. 2013, *ApJ*, 774, 26
 Chornock, R., Fox, D. B., Cucchiara, A., Perley, D. A., & Levan, A. 2014, *GCN*, 16301, 1
 Christensen, L., Møller, P., Fynbo, J. P. U., & Zafar, T. 2014, *MNRAS*, 445, 225
 Covino, S., Melandri, A., Salvaterra, R., et al. 2013, *MNRAS*, 432, 1231
 Cucchiara, A., Levan, A. J., Fox, D. B., et al. 2011a, *ApJ*, 743, 154
 Cucchiara, A., Cenko, S. B., Bloom, J. S., et al. 2011b, *ApJ*, 736, 7
 D'Avanzo, P., Perri, M., Fugazza, D., et al. 2010, *A&A*, 522, A20
 de Cia, A., Jakobsson, P., Björnsson, G., et al. 2011, *MNRAS*, 412, 2229
 de Cia, A., Ledoux, C., Fox, A. J., et al. 2012, *A&A*, 545, A64
 De Cia, A., Ledoux, C., Savaglio, S., Schady, P., & Vreeswijk, P. M. 2013, *A&A*, 560, A88
 de Ugarte Postigo, A., Fynbo, J. P. U., Thone, C. C., et al. 2012, *A&A*, 548, A11
 D'Elia, V., Fiore, F., Meurs, E. J. A., et al. 2007, *A&A*, 467, 629
 D'Elia, V., Fynbo, J. P. U., Covino, S., et al. 2010, *A&A*, 523, A36
 D'Elia, V., Fynbo, J. P. U., Goldoni, P., et al. 2014, *A&A*, 564, A38
 D'Elia, V., Campana, S., Covino, S., et al. 2011, *MNRAS*, 418, 680
 Eliásdóttir, Á., Fynbo, J. P. U., Hjorth, J., et al. 2009, *ApJ*, 697, 1725
 Elliott, J., Krühler, T., Greiner, J., et al. 2013, *A&A*, 556, A23
 Fenner, Y., Prochaska, J. X., & Gibson, B. K. 2004, *ApJ*, 606, 116
 Ferrero, P., Klose, S., Kann, D. A., et al. 2009, *A&A*, 497, 729
 Fiore, F., D'Elia, V., Lazzati, D., et al. 2005, *ApJ*, 624, 853
 Fox, A. J., Ledoux, C., Vreeswijk, P. M., Smette, A., & Jaunsen, A. O. 2008, *A&A*, 491, 189
 Freudling, W., Romaniello, M., Bramich, D. M., et al. 2013, *A&A*, 559, A96
 Friis, M., de Cia, A., Krühler, T., et al. 2014, arXiv:1409.6315
 Fumagalli, M., O'Meara, J. M., Prochaska, J. X., Kanekar, N., & Wolfe, A. M. 2014, *MNRAS*, 444, 1282
 Fumagalli, M., O'Meara, J. M., Prochaska, J. X., & Worseck, G. 2013, *ApJ*, 775, 78
 Fynbo, J. P. U., Geier, S. J., Christensen, L., et al. 2013, *MNRAS*, 436, 361
 Fynbo, J. P. U., Gorosabel, J., Smette, A., et al. 2005, *ApJ*, 633, 317
 Fynbo, J. P. U., Hjorth, J., Malesani, D., et al. 2008a, in Proc. of the MG11 Meeting on General Relativity, The Eleventh Marcel Grossmann Meeting On Recent Developments in Theoretical and Experimental General Relativity Gravitation and Relativistic Field Theories, ed. H. Kleinert, R. T. Jantzen, & R. Ruffini (Singapore: World Scientific), 726
 Fynbo, J. P. U., Hjorth, J., Malesani, D., et al. 2009, *ApJS*, 185, 526
 Fynbo, J. P. U., Hjorth, J., Malesani, D., et al. 2011, *MNRAS*, 413, 2481
 Fynbo, J. P. U., Prochaska, J. X., Sommer-Larsen, J., Dessauges-Zavadsky, M., & Møller, P. 2008b, *ApJ*, 683, 321
 Fynbo, J. P. U., Starling, R. L. C., Ledoux, C., et al. 2006, *A&A*, 451, L47
 Galama, T. J., Vreeswijk, P. M., van Paradijs, J., et al. 1998, *Natur*, 395, 670
 Gall, C., Hjorth, J., & Andersen, A. C. 2011, *A&ARv*, 19, 43
 Gehrels, N., Chincarini, G., Giommi, P., et al. 2004, *ApJ*, 611, 1005
 Goldoni, P., Royer, F., Royer, F., et al. 2006, in Proc. SPIE, 6269, 62692
 Graham, J. F., & Fruchter, A. S. 2013, *ApJ*, 774, 119
 Greif, T. H., Bromm, V., Clark, P. C., et al. 2012, *MNRAS*, 424, 399
 Grevesse, N., & Sauval, A. J. 1998, *SSRv*, 85, 161
 Hjorth, J., Malesani, D., Jakobsson, P., et al. 2012, *ApJ*, 756, 187
 Hjorth, J., Melandri, A., Malesani, D., Kruehler, T., & Xu, D. 2013, *GCN*, 14365, 1
 Hjorth, J., Møller, P., Gorosabel, J., et al. 2003b, *ApJ*, 597, 699
 Hjorth, J., Sollerman, J., Møller, P., et al. 2003a, *Natur*, 423, 847
 Hunt, L. K., Palazzi, E., Michalowski, M. J., et al. 2014, *A&A*, 565, A112
 Jakobsson, P., Chapman, R., Hjorth, J., et al. 2013, arXiv:1309.3988
 Jakobsson, P., Fynbo, J. P. U., Ledoux, C., et al. 2006, *A&A*, 460, L13
 Jakobsson, P., Hjorth, J., Fynbo, J. P. U., et al. 2004, *A&A*, 427, 785
 Jorgenson, R. A., Murphy, M. T., & Thompson, R. 2013, *MNRAS*, 435, 482
 Jorgenson, R. A., Murphy, M. T., Thompson, R., & Carswell, R. F. 2014, *MNRAS*, 443, 2783
 Jorgenson, R. A., & Wolfe, A. M. 2014, *ApJ*, 785, 16
 Karlsson, T., Bromm, V., & Bland-Hawthorn, J. 2013, *RvMP*, 85, 809
 Kawai, N., Kosugi, G., Aoki, K., et al. 2006, *Natur*, 440, 184
 Kistler, M. D., Yüksel, H., Beacom, J. F., Hopkins, A. M., & Wyithe, J. S. B. 2009, *ApJL*, 705, L104
 Kocevski, D., & West, A. A. 2011, *ApJL*, 735, L8
 Kocevski, D., West, A. A., & Modjaz, M. 2009, *ApJ*, 702, 377
 Krogager, J.-K., et al. 2013, *MNRAS*, 433, 3091
 Kröger, D., Hensler, G., & Freyer, T. 2006, *A&A*, 450, L5
 Krongold, Y., & Prochaska, J. X. 2013, *ApJ*, 774, 115
 Krühler, T., Fynbo, J. P. U., Geier, S., et al. 2012, *A&A*, 546, A8
 Krühler, T., Ledoux, C., Fynbo, J. P. U., et al. 2013, *A&A*, 557, A18
 Kulkarni, G., Rollinde, E., Hennawi, J. F., & Vangioni, E. 2013, *ApJ*, 772, 93
 Laskar, T., Berger, E., & Chary, R.-R. 2011, *ApJ*, 739, 1
 Lazzati, D., Perna, R., Flasher, J., Dwarkadas, V. V., & Fiore, F. 2006, *MNRAS*, 372, 1791
 Ledoux, C., Vreeswijk, P. M., Smette, A., et al. 2009, *A&A*, 506, 661
 Levan, A. J., Tanvir, N. R., Starling, R. L. C., et al. 2014, *ApJ*, 781, 13
 Levesque, E. M., Kewley, L. J., Berger, E., & Zahid, H. J. 2010, *AJ*, 140, 1557
 Mao, J. 2010, *ApJ*, 717, 140

- Matteucci, F., & Recchi, S. 2001, *ApJ*, **558**, 351
- Mészáros, P. 2013, *Aph*, **43**, 134
- Modjaz, M., Kewley, L., Kirshner, R. P., et al. 2008, *AJ*, **135**, 1136
- Neeleman, M., Wolfe, A. M., Prochaska, J. X., & Rafelski, M. 2013, *ApJ*, **769**, 54
- Noterdaeme, P., Laursen, P., Petitjean, P., et al. 2012b, *A&A*, **540**, A63
- Noterdaeme, P., Ledoux, C., Petitjean, P., & Srianand, R. 2008, *A&A*, **481**, 327
- Noterdaeme, P., Petitjean, P., Carithers, W. C., et al. 2012a, *A&A*, **547**, L1
- Noterdaeme, P., Petitjean, P., Ledoux, C., & Srianand, R. 2009, *A&A*, **505**, 1087
- Noterdaeme, P., Petitjean, P., Pâris, I., et al. 2014, *A&A*, **566**, A24
- Page, K. L., Willingale, R., Bissaldi, E., et al. 2009, *MNRAS*, **400**, 134
- Patel, M., Warren, S. J., Mortlock, D. J., & Fynbo, J. P. U. 2010, *A&A*, **512**, L3
- Penprase, B. E., Berger, E., Fox, D. B., et al. 2006, *ApJ*, **646**, 358
- Penprase, B. E., Prochaska, J. X., Sargent, W. L. W., Toro-Martinez, I., & Beeler, D. J. 2010, *ApJ*, **721**, 1
- Perley, D. A., Levan, A. J., Tanvir, N. R., et al. 2013, *ApJ*, **778**, 128
- Perley, D. A., Perley, R. A., Hjorth, J., et al. 2014, arXiv:1407.4456
- Péroux, C., McMahon, R. G., Storrie-Lombardi, L. J., & Irwin, M. J. 2003, *MNRAS*, **346**, 1103
- Pontzen, A., Deason, A., Governato, F., et al. 2010, *MNRAS*, **402**, 1523
- Price, P. A., Songaila, A., Cowie, L. L., et al. 2007, *ApJL*, **663**, L57
- Prochaska, J. X. 2006, *ApJ*, **650**, 272
- Prochaska, J. X., Chen, H.-W., & Bloom, J. S. 2006, *ApJ*, **648**, 95
- Prochaska, J. X., Chen, H.-W., Dessauges-Zavadsky, M., & Bloom, J. S. 2007, *ApJ*, **666**, 267
- Prochaska, J. X., Dessauges-Zavadsky, M., Ramirez-Ruiz, E., & Chen, H.-W. 2008, *ApJ*, **685**, 344
- Prochaska, J. X., Gawiser, E., Wolfe, A. M., Cooke, J., & Gelino, D. 2003, *ApJS*, **147**, 227
- Prochaska, J. X., Sheffer, Y., Perley, D. A., et al. 2009, *ApJL*, **691**, L27
- Prochaska, J. X., & Wolfe, A. M. 1996, *ApJ*, **470**, 403
- Prochaska, J. X., & Wolfe, A. M. 2009, *ApJ*, **696**, 1543
- Rafelski, M., Neeleman, M., Fumagalli, M., Wolfe, A. M., & Prochaska, J. X. 2014, *ApJL*, **782**, L29
- Rafelski, M., Wolfe, A. M., Prochaska, J. X., Neeleman, M., & Mendez, A. J. 2012, *ApJ*, **755**, 89
- Rau, A., Savaglio, S., Krühler, T., et al. 2010, *ApJ*, **720**, 862
- Reichart, D. E., & Price, P. A. 2002, *ApJ*, **565**, 174
- Ritter, J. S., Sluder, A., Safranek-Shrader, C., Milosavljevic, M., & Bromm, V. 2014, arXiv:1408.0319
- Robertson, B. E., & Ellis, R. S. 2012, *ApJ*, **744**, 95
- Ruiz-Velasco, A. E., Swan, H., Troja, E., et al. 2007, *ApJ*, **669**, 1
- Salvadori, S., & Ferrara, A. 2012, *MNRAS*, **421**, L29
- Salvaterra, R., Campana, S., Vergani, S. D., et al. 2012, *ApJ*, **749**, 68
- Salvaterra, R., della Valle, M., Campana, S., et al. 2009, *Natur*, **461**, 1258
- Sanchez-Ramirez, R., de Ugarte Postigo, A., Kruehler, T., et al. 2012, GCN, 14035, 1
- Savage, B. D., & Sembach, K. R. 1991, *ApJ*, **379**, 245
- Savaglio, S. 2006, *NJPh*, **8**, 195
- Savaglio, S. 2012, *AN*, **333**, 480
- Savaglio, S., & Fall, S. M. 2004, *ApJ*, **614**, 293
- Savaglio, S., Fall, S. M., & Fiore, F. 2003, *ApJ*, **585**, 638
- Savaglio, S., Fiore, F., Israel, G., et al. 2002, GCN, 1633, 1
- Savaglio, S., Rau, A., Greiner, J., et al. 2012, *MNRAS*, **420**, 627
- Schady, P., Savaglio, S., Krühler, T., Greiner, J., & Rau, A. 2011, *A&A*, **525**, A113
- Schmitt, J. H. M. M. 1985, *ApJ*, **293**, 178
- Schulze, S., Fynbo, J. P. U., Milvang-Jensen, B., et al. 2012, *A&A*, **546**, A20
- Shin, M.-S., Berger, E., Penprase, B. E., et al. 2006, arXiv:astro-ph/0608327
- Skuladóttir, A. 2010, Master thesis, Univ. Copenhagen
- Sparre, M., Hartoog, O. E., Krühler, T., et al. 2013, arXiv:1309.2940
- Sparre, M., Hartoog, O. E., Krühler, T., et al. 2014, *ApJ*, **785**, 150
- Spitzer, L. 1978, *Physical Processes in the Interstellar Medium* (New York: Wiley)
- Srianand, R., Gupta, N., Petitjean, P., et al. 2012, *MNRAS*, **421**, 651
- Starling, R. L. C., Rol, E., van der Horst, A. J., et al. 2009, *MNRAS*, **400**, 90
- Tanvir, N. R., Cucchiara, A., & Cenko, S. B. 2013, GCN, 14366, 1
- Tanvir, N. R., Fox, D. B., Levan, A. J., et al. 2009, *Natur*, **461**, 1254
- Tanvir, N. R., Levan, A. J., Fruchter, A. S., et al. 2012, *ApJ*, **754**, 46
- Tanvir, N. R., Levan, A. J., Wiersema, K., et al. 2014, GCN, 16150, 1
- Thöne, C. C., Kann, D. A., Jóhannesson, G., et al. 2010, *A&A*, **523**, A70
- Thöne, C. C., Fynbo, J. P. U., Goldoni, P., et al. 2013, *MNRAS*, **428**, 3590
- Trenti, M., Perna, R., & Jimenez, R. 2014, arXiv:1406.1503
- Trenti, M., Perna, R., & Tacchella, S. 2013, *ApJL*, **773**, L22
- Vergani, S. D., Salvaterra, R., Japelj, J., et al. 2014, arXiv:1409.7064
- Vladilo, G., Abate, C., Yin, J., Cescutti, G., & Matteucci, F. 2011, *A&A*, **530**, A33
- Vreeswijk, P. M., Ellison, S. L., Ledoux, C., et al. 2004, *A&A*, **419**, 927
- Vreeswijk, P. M., Smette, A., Fruchter, A. S., et al. 2006, *A&A*, **447**, 145
- Vreeswijk, P. M., Ledoux, C., Smette, A., et al. 2007, *A&A*, **468**, 83
- Vreeswijk, P. M., Ledoux, C., Raassen, A. J. J., et al. 2013, *A&A*, **549**, A22
- Watson, D., Fynbo, J. P. U., Ledoux, C., et al. 2006, *ApJ*, **652**, 1011
- Wolfe, A. M., Gawiser, E., & Prochaska, J. X. 2005, *ARA&A*, **43**, 861
- Wolfe, A. M., Lanzetta, K. M., Foltz, C. B., & Chaffee, F. H. 1995, *ApJ*, **454**, 698
- Woosley, S. E. 1993, *ApJ*, **405**, 273
- Woosley, S. E. 2011, arXiv:1105.4193
- Woosley, S. E., & Heger, A. 2006, *ApJ*, **637**, 914
- Woosley, S. E., & Heger, A. 2012, *ApJ*, **752**, 32
- Yoshida, N., Omukai, K., & Hernquist, L. 2008, *Sci*, **321**, 669
- Zafar, T., & Watson, D. 2013, *A&A*, **560**, A26